

RSC Advances

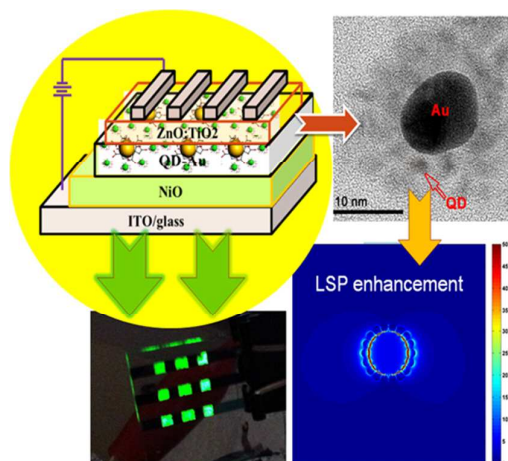


This is an *Accepted Manuscript*, which has been through the Royal Society of Chemistry peer review process and has been accepted for publication.

Accepted Manuscripts are published online shortly after acceptance, before technical editing, formatting and proof reading. Using this free service, authors can make their results available to the community, in citable form, before we publish the edited article. This *Accepted Manuscript* will be replaced by the edited, formatted and paginated article as soon as this is available.

You can find more information about *Accepted Manuscripts* in the [Information for Authors](#).

Please note that technical editing may introduce minor changes to the text and/or graphics, which may alter content. The journal's standard [Terms & Conditions](#) and the [Ethical guidelines](#) still apply. In no event shall the Royal Society of Chemistry be held responsible for any errors or omissions in this *Accepted Manuscript* or any consequences arising from the use of any information it contains.



We demonstrate quantum dot capped gold nanoparticle composite as emitting layer in quantum dot light-emitting diodes to achieve enhanced efficiency.

Cite this: DOI: 10.1039/c0xx00000x

www.rsc.org/xxxxxx

Full paper

Localized Surface Plasmon Resonance Enhanced Quantum Dot Light-emitting Diodes via Quantum Dot-capped Gold Nanoparticles

Jing Chen^{1§}, Qianqian Huang^{1§}, Qing Guo Du², Dewei Zhao^{3*}, Feng Xu¹, Jiangyong Pan¹, Wei Lei^{1*}, and Arokia Nathan⁴

Received (in XXX, XXX) XthXXXXXXXXXX 20XX, Accepted Xth XXXXXXXXXXXX 20XX

DOI: 10.1039/b000000x

The coupling of localized surface plasmon resonance (LSPR) and excitons in nanomaterials can improve the performance of nano-optoelectronic devices. We synthesized quantum dot (QD) capped gold (Au) nanoparticle (NP) composite used as emitting layer in all inorganic quantum dot light-emitting diodes (QD-LEDs). The photoluminescence (PL) peak of QD is fully overlapped with the absorption peak of Au NPs to realize the maximum LSPR enhancement. The LSPR effect of QD-capped Au NPs has been demonstrated by increased radiative emission, PL excitation intensity, and reduced exciton lifetime carried out by time-resolved PL measurement. As a result, quantum yield of 60% for QD-capped Au NPs has been realized and QD-LED has achieved remarkably enhanced power efficiency of 6.2 lm/W and maximum brightness of 1005 cd/m² after various optimization conditions. These results demonstrate that QD-capped Au NPs constitute an effective route for achieving high-performance optoelectronic devices.

1. Introduction

Quantum dot light-emitting diodes (QD-LEDs) have attracted much attention in the past few years since they possess unique properties of tunable emission wavelengths by controlling the size of QDs, high color saturation, narrow full width at half maxima (FWHM), solution process, and compatibility with flexible substrates¹. In order to realize high-performance QD-LEDs, it is necessary to explore novel materials technology, device configurations, and new emitting materials. The use of inorganic nanomaterials as the charge transport layer instead of organic semiconductors, such as ZnO², TiO₂³, NiO⁴, and WO₃⁵, opens the door to flexible, large-area, and stable QD-LEDs; on the other hand, the conventional emitting semiconductors, including CdSe/ZnS¹, ZnSe⁶, CuInSe₂⁷, CdTe⁸, CdSe/CdS/ZnS⁹, and novel hybrid nanomaterials, such as QD-metal composites, play a very important role in improving device performance of optoelectronic devices due to nano-scaled architecture.

Recently, localized surface plasmon resonance (LSPR) enhanced LED has been widely studied to break through the bottleneck on the performance for displays application¹⁰. The mechanism behind is the coupling effect between excitons and surface plasmons, which results from the overlap of local electromagnetic field of excitons in the emissive layer and surface plasmons, leading to significant radiative emission through effective energy transfer in LEDs¹⁰. As reported previously, LSPR enhanced LEDs fabricated by incorporating noble metallic nanoparticles (NPs) film into LEDs open up a new class of highly efficient solid-state light sources¹¹. The type, shape, height, and density of the metal NPs determine the degree of device performance enhancement. It is found that the

fluorescence increases as high as 30-fold for the QD film deposited on a triangular gold array fabricated by electron beam lithography (EBL) method¹². However, the cost of device fabrication is so expensive due to complex processing, restricting the widespread use and commercialization of the technology. On the contrary, a low-cost and large-area fabrication using solution process has attracted great attention for LSPR enhanced LEDs based on QD-metal hybrid. Carbon-dot supported silver NPs are used for achieving highly efficient polymer LEDs with a luminous efficiency of 18.54 lm/W, which is ascribed to the LSPR-induced enhancement¹⁰.

In this work, we present a novel, simple, and facile technique for the synthesis of ZnCdSeS QD-capped gold (Au) NP hybrids. We also investigate the LSPR enhanced optical properties of the hybrid nanomaterials in terms of experiments and simulation. To demonstrate the potential applications of the ZnCdSeS QD-capped Au NPs in optoelectronic devices, an all-inorganic QD-LED with multiple layers was fabricated by a simple solution method, and exhaustively evaluated.

2. Experimental Section

Preparation of QD-capped Au NPs hybrid: The high-quality green emitting ZnCdSeS QDs were synthesized according to a method reported in the literature¹³. As a typical synthetic procedure, 0.4 mmol of CdO, 4 mmol of zinc acetate, 15.5 mmol of oleic acid (OA), and 30 mL of 1-octadecene were placed in a 100 mL round flask. The mixture was heated up to 150 °C and degassed for 30 min, and further heated up to 310 °C to form a clear solution of Cd(OA)₂ and Zn(OA)₂ at high-purity N₂ atmosphere. At this temperature, a stock solution containing 4 mL of trioctylphosphine, 0.4 mmol of Se, and 4 mmol of S was

quickly injected into the reaction flask. After the injection, the reaction temperature was kept for 10 min to promote the growth of QDs, and then cooled down to room temperature to stop the growth. QDs were washed with acetone for three times, and finally dispersed in chloroform at the concentration of 10 mg/ml.

The Au solution was prepared as reported¹⁴. After that, QDs were transferred into Au aqueous solution and the process is as follows. 5 mL of QDs in chloroform dispersed in mixed chloroform: thioglycolic acid (TGA) (50 mL: 10 mL) was added to the solution. The resulting reaction mixture was heated up to 60 °C for 1 h and cooled down to room temperature. The TGA-capped QDs were extracted by centrifugation at 6500 rpm. The TGA-capped QDs were mixed with Au aqueous solution, and the pH value was adjusted to 7~10 by adding tetramethylammonium hydroxide (TMAOH), which was shaken for a period in order to form QD-capped Au product. Finally, the solution with 10 mg/mL concentration of QD-capped Au was dispersed into H₂O: ethanol mixture (1:1 vol %). The photoluminescence quantum yields (PLQYs) of the NCs were measured and estimated by comparing their fluorescence intensities with those of primary standard dye solutions (rhodamine 6G, QY=95% in ethanol) at the optical density of below 0.05 at the same excitation wavelength (480 nm).

Device Fabrication: ITO glass substrate with a sheet resistance of about 20Ω/square was cleaned by successive ultrasonic treatments in detergent, de-ionized water, acetone, and isopropanol for 15 min, respectively, followed by ultraviolet ozone treatment for 30 min. NiO film was fabricated according to the previous report¹⁵, which was used as hole transport layer (HTL) with the thicknesses of 50 nm. The emissive layer of colloidal ZnCdSeS QDs-capped Au was spin-coated on HTL (1000 rpm, 30 s) and annealed at 120 °C for 30 min. Then a sol-gel ZnO:TiO₂ solution was deposited onto QDs layer (4000 rpm, 30 s) and annealed at 150 °C in air¹⁶. Finally, a 100 nm aluminium (Al) electrode was thermally evaporated under high vacuum (4×10⁻⁶Torr) on top of ZnO: TiO₂ ETL, followed by post-annealing at 100 °C for 20 min. The active area of the devices was defined by a shadow mask of 4 mm². The devices are named as sample A and B with QD and QD-capped Au as emitting layer, respectively.

Sample and Device characterization: The thicknesses of all films were measured by using Filmetrics F20-EXR. The current density-voltage (J-V) characteristics were measured with Keithley-2400 source-meter and electroluminescence (EL) spectra were recorded with Ocean Optics Maya 2000-PRO spectrometer. The absorption and photoluminescence (PL) spectra were measured by U-4100 UV-visible and NIR-300 spectrophotometer, respectively. Luminance-current density-voltage (L-J-V) curves were measured using a system incorporated with a Konica-Minolta CS-200 ChromaMeter. The structural analysis of the samples was carried out using a Cs-corrected high-resolution transmission electron microscope (HRTEM, Titan 80-300, FEI, U.S.A.) with an information limit 15 of 80 pm operated at an acceleration voltage of 300 kV. The TEM was equipped with a multiscan charge-coupled device (CCD) camera system (Model 894, Gatan, USA) to record the HRTEM images.

3. Results and discussion

The chemical synthesis processes for the ZnCdSeS QD-capped Au NP composites are summarized graphically in Fig. 1. ZnCdSeS QDs are dispersed in aqueous solution by exchanging ligand from oleic acid to TGA, as shown in Fig. 1(a). The Au NPs were negatively charged due to the citrate ions adsorbed on the surface of Au NPs, as shown in Fig. 1(b). Therefore, the QDs are bonded with Au NPs via ionic interaction because the QDs were positively charged while Au NPs were negatively charged¹⁴, as shown in Fig. 1(c). Fig. 1(d) shows the photo of a vial of ZnCdSeS capped Au aqueous solution, separated from chloroform, exhibiting green emission under 365 nm excitation light.

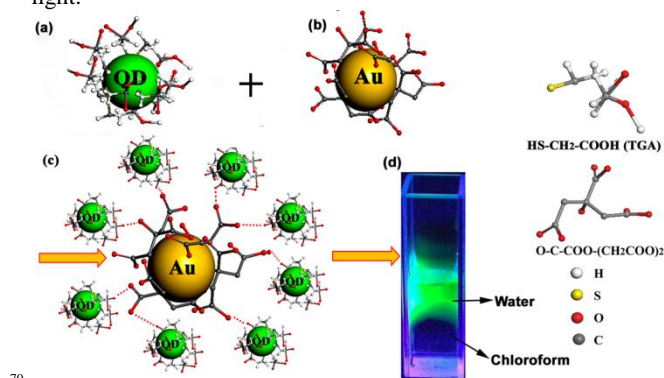


Fig. 1. (a) Schematic of ZnCdSeS QD capped TGA after ligand exchanging. (b) Schematic of Au capped by citrate. (c) QD capped Au via ionic interaction. (d) Photo of a vial of ZnCdSeS capped Au aqueous solution, separated from chloroform, exhibiting green emission under 365 nm excitation light. The magnified ligands show TGA and citrate capped QD and Au.

It is observed that the ratio of QD to Au and pH value of the hybrid solution have significant effect on the PL intensity, as shown in Fig. 2(a) and (b). As the volume ratio of QD to Au reduced, the PL intensity firstly increased to the maximum value and then decreased. When the ratio of QD to Au was adjusted to 16.7:1, the PL can reach the maximum value. There are two competing processes: LSPR and fluorescence (Förster) resonance energy transfer (FRET) process in QD-Au system¹⁴. The LSPR process can be able to result in a more effective QD excitation and FRET process causes the fluorescence quenching. When the amount of Au NP is low, the LSPR process is dominated, leading to the enhancement of PL intensity. On the other hand, at a high amount of Au NPs, FRET process is dominated, resulting in the quenching of PL intensity¹⁴. Meanwhile, the pH value also plays an important role in LSPR enhancement. PL intensity is stable until pH value reaches 9~10. The reason is that thioglycolic acid is a liquid with a pK_{a1}(-COOH) ranging from 3.55 to 3.82 and pK_{a2}(-SH) from 9.30 to 10.23¹⁷. As the pH value is higher than 9, the thiol group (-S) anchored to QD is more stable, leading to the increased PL intensity of QD-Au composite. Fig. 2(c) presents the TEM image of Au NPs dispersed in water with an average diameter of 20 nm. The HRTEM image, as shown in Fig. 2(d), indicates that ZnCdSeS QDs were uniformly dispersed in water with an average diameter of ~4 nm. Fig. 2(e) and 2(f) show the HRTEM images of QD-capped Au NPs with the ratio of QD to Au of 16.7:1, and the pH value of 9~10. The Au NP was found to be surrounded by ZnCdSeS QDs, which is the evidence of the

ligand bonding between QD and Au NP. Close-packed monolayers of QDs can be produced on the substrate after the solvent evaporation, and the QD-Au hybrid follows a similar trend¹⁸, as shown in Fig. 2(e). However, Au NP was observed to be capped by monolayer QD after the hybrid solution was diluted. It is inferred that the chemical reaction only occurs between QDs and Au NPs, not among QDs.

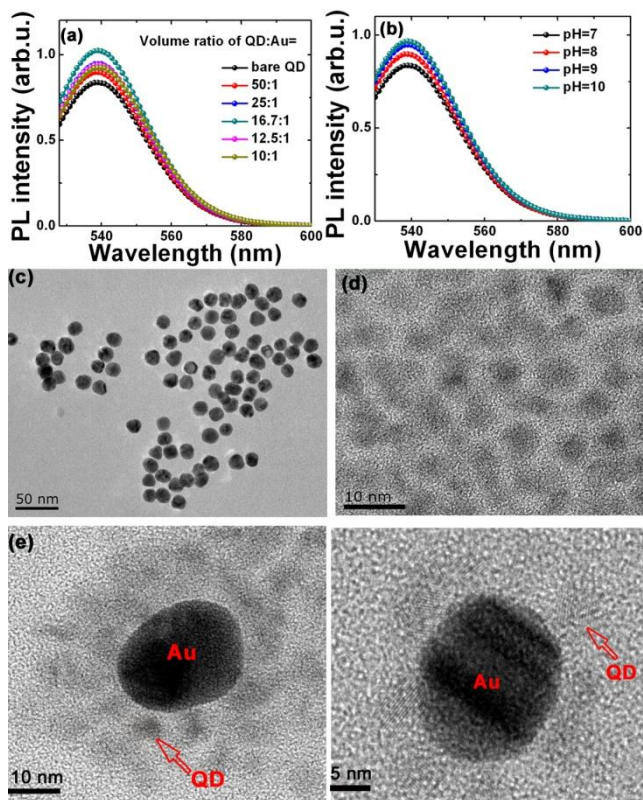


Fig. 2. LSPR enhancement process depends on a) the ratio of QD and Au NPs, and b) pH value of QD capped Au solution. (c) TEM image of Au NPs. (d) HRTEM image of pristine QDs. (e) and (f) QD-capped Au NPs.

Fig. 3(a) shows the absorption and PL spectra of Au NPs, ZnCdSe QDs, and ZnCdSe QD capped Au NPs in aqueous solution. The ratio of QD and Au is fixed at 16.7:1 and the pH value is 9~10. The absorption spectra clearly display the first excitonic transition peaks at 520 nm and 522 nm for QD and Au NP, respectively. Meanwhile, the PL spectrum shows a Gaussian-shaped peak located at 538 nm with a narrow FWHM of 30 nm for QDs and QD-Au NPs. The LSPR enhancement will be maximized when the excitation energy is close to the LSPR absorption peak of Au NPs¹⁴. It is found that the PL intensity is enhanced for the QDs at the presence of Au NPs, implying that an interaction between QDs and Au NPs exists due to the LSPR from Au NPs. Meanwhile, according to the rhodamine 6G reference and the area of PL curves in Fig. 3(a), the PL QY of QDs with TGA at room temperature was 48%; while that of QD-Au NPs with TGA was increased to 60%.

According to the TEM results, there are many possibilities regarding the number of QD-Au NPs that can be formed; accordingly, we performed the simulation using the three-dimensional finite-difference time-domain (FDTD) method by varying the number of QD-Au NPs (from 1 to 4) [Fig. S2 (ESI)[†]].

The electric field enhancement as high as 100 fold at the gap can be obtained between the Au NPs and the surface of Au. Thus, the simulation demonstrates that the QD-Au hybrid structure can enhance the PL intensity due to LSPR effect.

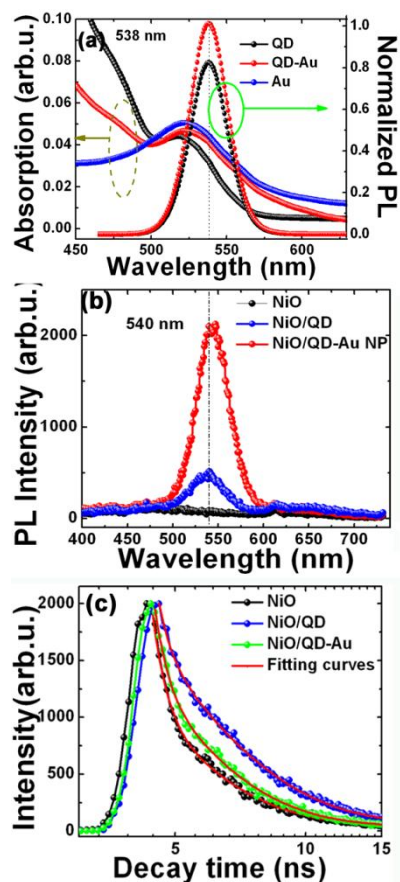


Fig. 3. (a) Absorption spectra and PL spectra excited under 480 nm. (b) PL spectra of NiO/QD film and NiO/QD-Au film. (c) TRPL spectra of NiO/QD film and NiO/QD-Au film with fitting curves excited under a 325 nm laser source.

Fig. 3(b) shows the PL spectra of the films composed of QDs with and without Au NPs deposited on NiO as HTL. Obviously, the PL intensity of the NiO/QDs-Au film is 4-5 times higher than that of the NiO/QDs film at the excitation wavelength of 325 nm due to the LSPR enhancement. To further elucidate the decay dynamics of QD-capped Au NPs, we carried out time-resolved PL (TRPL) measurements. The TRPL spectra of films prepared by pristine QDs and QD-capped Au NPs are shown in Fig. 3(c). It is obvious that the exciton lifetime is reduced upon the incorporation of Au NPs. The average exciton lifetimes of NiO/QDs-Au and NiO/QDs are estimated to be 2.3 and 3.2 ns, respectively (Table. S1, ESI)[†]. Therefore, TRPL measurement provides the direct evidence of the enhanced spontaneous emission rate of QDs induced by LSPR on Au NPs, which can be ascribed to near-field enhancement. Meanwhile, the spherical shape of Au NPs could result in the high electric field intensity distribution around Au NPs [Fig. S2 (ESI)[†]], which facilitates to extract the LSPR energy as light and thereby enhances the electroluminescence (EL) intensity¹⁹.

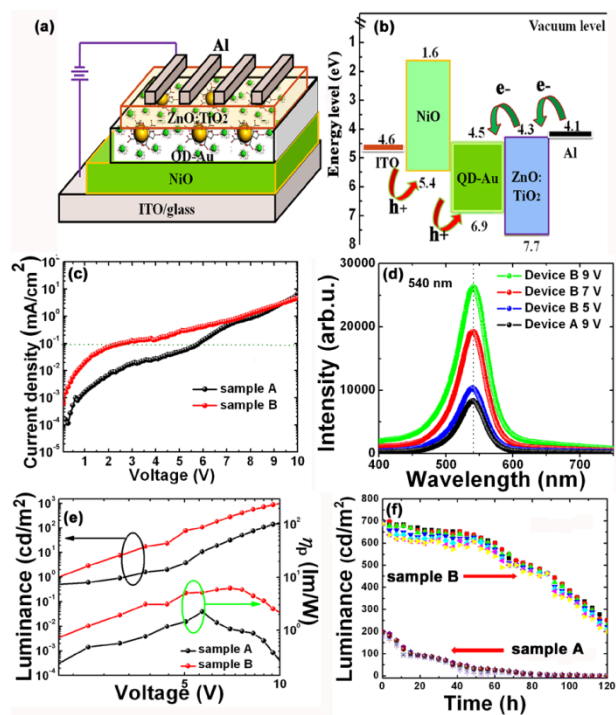


Fig. 4. (a) Schematic of the device structure. (b) The corresponding energy band diagram of a plasmonic QD-LED. (c) Current density versus driving voltage. (d) The EL spectra of sample A at the voltage of 9 V and sample B at the voltage varying from 5-9 V. (e) Luminance versus driving voltage and power efficiency versus driving voltage. (f) Luminance versus operating time for sample A and B.

The schematics of our device structure and corresponding energy level diagram are shown in Fig.4 (a) and (b). The device consists of patterned ITO as anode, a 50 nm NiO layer as HTL, a 30 nm QD layer as emissive layer with 3 to 4 closely packed QD-capped Au NP monolayers, a 40 nm ZnO: TiO₂ layer as ETL, and a 100 nm Al layer as cathode. The concentration of QDs is 10 mg/ml with the ratio of QD to Au of 16.7:1, and the pH value of 9~10.

The all-inorganic QD-LED structure was designed to achieve efficient electron and hole injection from the electrodes to the QD layer. More importantly, NiO and ZnO effectively block electrons and holes from passing through the QD-Au layer in terms of the energy levels of the constituent layers [Fig. 4(b)]. The optical bandgap of hybrid ZnO: TiO₂ is determined as 3.4 eV and QD capped Au is calculated as 2.39 eV. A small injection step of 0.4 eV exists for the injection of electrons from Al to the QD layer since the hybrid ZnO: TiO₂ has an electron affinity of 4.3 eV, slightly higher than the work function of Al (4.1 eV). On contrast, the barrier between valance bands (VBs) of NiO and QDs is higher than 1 eV. However, it is reported that the barrier for hole injection is much smaller (~0.1-0.5 eV) since the ionization energy of QD was measured to be 1 eV shallower than that derived from the value of ultra violet photoelectron spectroscopy measurement (6.5-6.9 eV)²⁰. Meanwhile, the conduction band (CB) of NiO can effectively block injected electrons, confining the charges within the QD layer. Compared to the conventional HTL PEDOT: PSS with an HOMO of 5.0 eV and a LUMO of 3.4 eV, the hole injection of NiO is expected to be better than that of PEDOT: PSS. The surface morphology and roughness of NiO and QD-capped Au revealed by AFM images are measured as 3.5 nm and 2.5 nm, respectively (Fig. S3, ESI)

†.Therefore, the QD-LED architecture described here has been demonstrated to facilitate the transport of holes and electrons into the QD-capped Au layer.

Fig. 4(c) shows the current density-voltage (J-V) of sample A and B under forward bias. The devices exhibit low turn-on voltage of 2.6 V for sample B and 5.6 V for sample A. Fig. 5(d) compares the EL spectra of sample B at 5, 7, and 9 V and that of sample A at 9 V. It can be seen that the emission intensity for sample B at 528 nm increases with the driving voltage, which is as nearly 4-fold high as that for sample A. Fig. 5(a)-(c) shows the photos of operating devices for sample A and sample B with the Commission Internationale de l'Enclairage (CIE) coordinates, shown as Fig.5(d). The color of sample A is inside the NTSC standard color triangle, while sample B lies outside but near it. Compared to sample A, the color of sample B is more saturated, which is located outside the National Television System Committee (NTSC) color standards. The EL emission for identical QDs exhibits a slight red shift, compared with the PL emission (as shown in Fig. 3a), likely attributed to the inter-dot interaction, as observed previously in closely packed QD solids, and also likely attributed to the electric-field-induced Stark effect^{4,20}.

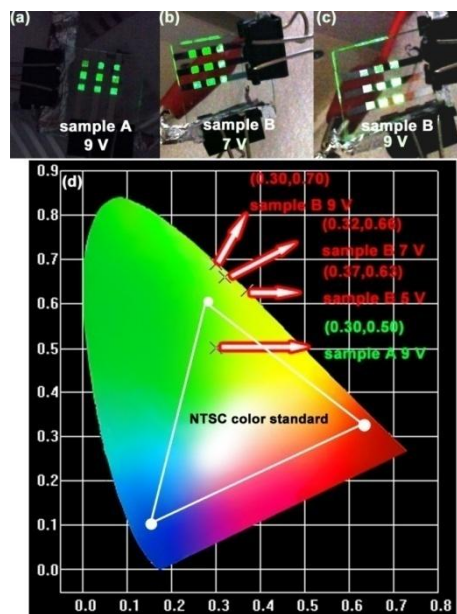


Fig.5. (a)-(c) CIE coordinates of sample A and B under different applied voltage with (d) the National Television System Committee (NTSC) color standards (circle).

Fig. 4(e) shows the brightness and power efficiency of samples A and B. Sample A has the maximum power efficiency of 2.22 lm/W. However, sample B obtains the maximum power efficiency of 6.2 lm/W and the maximum brightness of 1005 cd/m². The stability of the unencapsulated samples A and B at 10 mA/cm² is shown in Fig. 4(f) with repeated testing of 8 times. The lifetime for sample A is reduced sharply. After operation for 80 h, the luminance decreases by 29% for sample B; however, the luminance of sample A is totally degraded.

As discussed above, the reason for improving the performance of device is attributed to the increased QY value of QD-Au hybrid and the faster electron transfer rate in plasmonic QD-LED. Expect for that, coupling effect between excitons and

surface plasmons leads to significant radiative emission via effective energy transfer in organic LED (OLED)²¹ and polymer LED (PLED)^{10, 22}. In addition, for the hybrid emitter, the enhanced luminance of QD-LED is originated from the enhanced optical gain caused by the SPR effect of the hybrid¹⁰.

Conclusions

In summary, we have demonstrated, the solution-processed stable LSPR enhanced QD-LED by using ZnCdSeS QD capped Au NPs as green emitters. The proposed LSPR enhanced nanostructure is designed by using Au NPs, densely surrounded by compacted QDs, whose PL peak is overlapped with the absorption peak of Au NPs. This hybrid is beneficial for LSPR enhancement because the lifetime of TRPL is reduced and PL intensity for QD-capped Au NP is enhanced. LSPR enhancement is affected by as the position of QD and Au, the concentration ratio of QD to Au NPs, and pH value of QD-Au hybrid solution. After optimization of QD and Au NP, nearly 3-fold enhancement in the power efficiency of QD-LED has been achieved. Our results offer a promising approach for further developing high-efficiency and stable LSPR enhanced QD-LEDs using all inorganic materials.

Acknowledgments

This work was supported partially by the National Key Basic Research Program 973 (2013CB328804, 2013CB328803, and 2010CB327705), the National High-Tech R&D Program 863 of China (2012AA03A302, 2013AA011004) National Natural Science Foundation Project (51002031, 61007036, 61101023, 51202028, 61106055, 51372039, and 61271053), Foundation of Doctoral Program of Ministry of Education under Grant (20120092120025) and Natural Science Foundation of Jiangsu Province of China (BK20141390).

Notes and references

^aSchool of Electronic Science and Engineering, Southeast University, Nanjing, China, 210096; E-mail: lw@seu.edu.cn

^bInstitute of High Performance Computing, Singapore, 138632

^cDepartment of Electrical Engineering and Computer Science, the University of Michigan, Ann Arbor, Michigan 48109, USA; E-mail: dewei.zhao@hotmail.com

^dElectrical Engineering Division, Engineering Department, University of Cambridge, 9 JJ Thomson Avenue, CB3 0FA, Cambridge, UK

† Electronic Supplementary Information (ESI) available: [PL excitation (PLE) measurements, PL measurements, AFM images, CIE coordinates of sample A and B]. See DOI: 10.1039/b000000x/

[§] These authors contributed equally to this work.

1. L. Qian, Y. Zheng, J. Xue and P. H. Holloway, *Nat Photon*, 2011, **5**, 543-548.
2. J. W. Stouwdam and R. A. J. Janssen, *Journal of Materials Chemistry*, 2008, **18**, 1889-1894.
3. K. Qasim, J. Chen, Z. Li, W. Lei and J. Xa, *Rsc Advances*, **3**, 12104-12108.
4. J. M. Caruge, J. E. Halpert, V. Bulovic and M. G. Bawendi, *Nano Lett.*, 2006, **6**, 2991-2994.
5. X. Yang, E. Mutlugun, Y. Zhao, Y. Gao, K. S. Leck, Y. Ma, L. Ke, S. T. Tan, H. V. Demir and X. W. Sun, *Small*, 2014, **10**, 246-246.
6. A. Aharoni, T. Mokari, I. Popov and U. Banin, *Journal of the American Chemical Society*, 2006, **128**, 257-264.

7. H. Z. Zhong, Z. B. Wang, E. Bovero, Z. H. Lu, F. van Veggel and G. D. Scholes, *Journal of Physical Chemistry C*, **115**, 12396-12402.
8. E. Tekin, P. J. Smith, S. Hoepfner, A. M. J. van den Berg, A. S. Susha, A. L. Rogach, J. Feldmann and U. S. Schubert, *Advanced Functional Materials*, 2007, **17**, 23-28.
9. W. Ji, P. Jing, J. Zhao, X. Liu, A. Wang and H. Li, *Nanoscale*, 2013, **5**, 3474-3480.
10. H. Choi, S.-J. Ko, Y. Choi, P. Joo, T. Kim, B. R. Lee, J.-W. Jung, H. J. Choi, M. Cha, J.-R. Jeong, I.-W. Hwang, M. H. Song, B.-S. Kim and J. Y. Kim, *Nat Photon*, 2013, **7**, 732-738.
11. X. Gu, T. Qiu, W. Zhang and P. Chu, *Nanoscale Research Letters*, 2011, **6**, 199.
12. P. P. Pompa, M. Martiradonna, A. D. Torre, F. D. Sala, Manna, M. De Vittorio, Calabi, F. Cingolani, R. and Rinaldi, *Nat Nano*, 2006, **1**, 126-130.
13. W. K. Bae, K. Char, H. Hur and S. Lee, *Chem. Mat.*, 2008, **20**, 531-539.
14. L.-H. Jin, S.-M. Li, B.-J. Kwon and Y.-H. Cho, *Journal of Applied Physics*, 2011, **109**, 124310.
15. B. S. Mashford, T.-L. Nguyen, G. J. Wilson and P. Mulvaney, *Journal of Materials Chemistry*, 2009, **20**, 167-172.
16. J. Chen, D. Zhao, C. Li, F. Xu, W. Lei, L. Sun, A. Nathan and X. Sun, *Sci. Rep.*, 2014, **4**, 4085.
17. Oecd, in *SIDS Initial Assessment Report For SIAM 28: Thioglycolic acid and its ammonium salt*, United Nations Environment Programme, Paris, France, 2009.
18. C. B. Murray, C. R. Kagan and M. G. Bawendi, *Science*, 1995, **270**, 1335-1338.
19. Y. Xiao, J. P. Yang, P. P. Cheng, J. J. Zhu, Z. Q. Xu, Y. H. Deng, S. T. Lee, Y. Q. Li and J. X. Tang, *Applied Physics Letters*, 2012, **100**, -.
20. B. S. Mashford, M. Stevenson, Z. Popovic, C. Hamilton, Z. Q. Zhou, C. Breen, J. Steckel, V. Bulovic, M. Bawendi, S. Coe-Sullivan and P. T. Kazlas, *Nature Photonics*, 2013, **7**, 407-412.
21. A. Kumar, R. Srivastava, P. Tyagi, D. S. Mehta and M. N. Kamalasanan, *Organic Electronics*, 2012, **13**, 159-165.
22. J. H. Park, Y. T. Lim, O. O. Park, J. K. Kim, J. W. Yu and Y. C. Kim, *Chemistry of Materials*, 2004, **16**, 688-692.